Available online at www.sciencedirect.com
SCIENCE DIRECT
ELSEVIER
Colloids and Surfaces A: Physicochem. Eng. Aspects 282–283 (2006) 348–359
COLLOIDS AND SURFACES A
www.elsevier.com/locate/colsurfa

Foam sweep in fractures for enhanced oil recovery

Wei Yan, Clarence A. Miller, George J. Hirasaki *

MS-362, Rice University, Chemical and Biomolecular Engineering Department, 6100 Main Street, Houston, TX 77005, USA

Received 29 October 2005; received in revised form 23 February 2006; accepted 24 February 2006
Available online 18 April 2006

Dedicated to Professor Ivan B. Ivanov (LCPE, University of Sofia) on the occasion of his 70th birthday.

Abstract

A theory for foam flow in a uniform fracture was developed and verified by experiment. The apparent viscosity was found to be the sum of contributions arising from liquid between bubbles and the resistance to deformation of the interfaces of bubbles passing through the fracture. Apparent viscosity increases with gas fractional flow and is greater for thicker fractures (for a given bubble size), indicating that foam can divert flow from thicker to thinner fractures. This diversion effect was confirmed experimentally and modeled using the above theory for each individual fracture. The amount of surfactant solution required to sweep a heterogeneous fracture system decreases greatly with increasing gas fractional flow owing to the diversion effect and to the need for less liquid to occupy a given volume when foam is used.

Keywords: Foam; Bubbles; Fractures; Homogeneous; Heterogeneous; Apparent viscosity; Sweep

1. Introduction

Foam in porous media is a dispersed gaseous phase within a continuous aqueous phase comprised mainly of thin films known as lamellae. The lamellae are stabilized by adsorption of surfactant at the gas/liquid interfaces [1].

Because foam has an effective viscosity much higher than that of gas, it has been investigated as a method for improving sweep efficiency in processes where gases such as steam or supercritical CO_2 are injected to improve oil recovery from underground formations. Foam can reduce viscous fingering and gravity override caused by the low viscosity and density of the gas. Moreover, since fluids flow preferentially into layers of high permeability in a heterogeneous formation, foam is preferentially formed there and greatly increases local resistance to flow, thereby diverting injected fluids to zones of lower permeability and improving process efficiency.

The same potential advantages of using foam exist for surfactant and alkaline/surfactant processes for enhanced oil recovery except that gravity override is a less serious problem when surfactant solutions are injected. An additional advantage is that surfactant is already used in the basic process, so that additional chemical costs are low. One laboratory study of the possible use of foam in such processes for oil recovery and one successful field test by alkaline/surfactant/polymer/foam flooding have been reported [2,3]. Foam was used successfully a few years ago to improve sweep efficiency in a field test of a surfactant process for removing a chlorinated solvent from a sandy ground water aquifer [4]. Subsequently, the process was applied successfully to the remaining contaminated panels.

In this paper, we consider foam to improve efficiency of a surfactant process for oil recovery in a reservoir consisting of multiple fractures separating matrix blocks where oil is retained by capillarity and/or wettability. The injected surfactant solution enters the fractures, from which it penetrates the matrix blocks to release the oil. For instance, Hirasaki and Zhang [5] showed in a laboratory study that a solution of anionic surfactants in an alkaline solution could alter wettability and reduce interfacial tension in a matrix sample from a carbonate reservoir, releasing oil to flow upward by gravity into the fractures, where it could be directed toward production wells. But fracture systems have a broad distribution of fracture thicknesses. The thicker fractures will act as thief zones for the injected fluid. As a result, little of it will reach the thinner fractures. Foam provides a means to increase resistance to flow in the thicker

* Corresponding author. Tel.: +1 713 348 5416; fax: +1 713 348 5478.
E-mail address: gjh@rice.edu (G.J. Hirasaki).

0927-7757/$ – see front matter © 2006 Elsevier B.V. All rights reserved.
doi:10.1016/j.colsurfa.2006.02.067

Nomenclature

b	fracture aperture
b_i	aperture of fracture i
D_B	equivalent bubble diameter
FWR	foam-water ratio
f_g	gas fractional flow
K	crowding factor
K_I	internal circulation effect factor
k_i	permeability of fracture i
L	length of fractures
l	layer number
M_i	mobility ratio in fracture i
N	number of swept fractures
N_L	total number of fractures
∇p	pressure gradient
Δp	pressure difference
$\Delta p_{dynamic}$	dynamic pressure drop
PV	pore volume
LPV	injected liquid pore volume
Q_i	flow rate in fracture i
R	capillary radius
r_B	equivalent bubble radius
r_c	radius of curvature
Re	reynolds number
TPV	total pore volume
U	velocity of bubbles
V	aperture variance
v_i	velocity in layer
w_i	width of fracture i
x_i	dimensionless front of foam in fracture i
z_i	dimensionless hypothetical front of foam outside fracture i
σ	surface tension
ϕ	volume fraction
ϕ_{max}	dense random packing limit volume fraction
ρ^{liq}	density of liquid
μ_{app}	total apparent viscosity
$\mu_{app,i}$	apparent viscosity of displacing fluid in fracture i
μ_{app}^{liq}	apparent viscosity from liquid contribution
μ^{liq}	viscosity of pure fluid
μ_c	viscosity of continuous phase
μ_d	viscosity of dispersed phase
μ_i	apparent viscosity of fluid in fracture i
μ_r	relative viscosity
μ_{shape}^{liq}	apparent viscosity from bubble deformation

fractures and divert injected surfactant solution to the thinner fractures.

Two kinds of heterogeneous systems have been used in previous laboratory studies to investigate the ability of foam to improve sweep efficiency in parallel cores with differing permeabilities. The cores can be either isolated or placed in contact where cross flow can occur, e.g., in composite cylindrical cores. As indicated below, some of the studies have dealt with gas injection, others with injection of acid solutions to increase permeability.

Casteel and Djabbarah [6] used two parallel Berea cores with a 6.4 permeability ratio. They compared the use of foam with the water-alternating-gas process and showed that foam was preferentially generated in the more permeable core and could divert CO_2 towards the less permeable core. Llave et al. [7] obtained similar results with parallel cores with a 4.6 permeability ratio. Zerhboub et al. [8] studied matrix acidizing in a stratified system. They also showed clearly the effect of foam diversion. All these experiments, performed with parallel cores, considered only the case of porous media, which were not in capillary contact, so that crossflow was prohibited.

Yaghoobi et al. [9] used a short composite cylindrical core to study the influence of capillary contact. They observed a reduction of mobility in the higher permeability zone and called it "SMR", selective mobility reduction.

Siddiqui et al. [10] investigated the diversion characteristics of foam in Berea sandstone cores of contrasting permeabilities. They found that the diversion performance strongly depended on permeability contrast, foam quality and total flow rate.

Bertin et al. [11] studied foam propagation in an annularly heterogeneous porous medium having a permeability ratio of approximately 70. Experiments were performed with and without crossflow between the porous zones. In situ water saturations were measured continuously using X-ray computed tomography. They observed that foam fronts moved at the same rates in the two porous media if they were in capillary contact. On the other hand, when crossflow was prohibited due to the presence of an impervious zone between the layers, gas was blocked in the high permeability zone and diverted towards the low permeability core.

Osterloh and Jante [12] identified two distinct foam-flow regimes: a high-quality (gas fractional flow) regime in which steady-state pressure gradient is independent of gas flow rate, and a low-quality regime, in which steady-state pressure gradient is independent of liquid flow rate. In each regime foam behavior is dominated by a single mechanism: at high qualities by capillary pressure and coalescence [12], and at low qualities by bubble trapping and mobilization [13]. Cheng et al. [14] found that foam diversion is sensitive to permeability in high quality regime and insensitive to permeability in low quality regime. But in the low quality regime the harmful effect on diversion from crossflow is much less.

Nguyen et al. [15] conducted experiments to study foam-induced fluid diversion in isolated and capillary-communicating double layer cores. They found that there existed a threshold injection foam quality below which foam no longer invaded the low permeability layer. This threshold depends on the permeability contrast and foam strength in the high permeability layer. The use of foam below the threshold quality is appropriate in foam acid diversion, where the presence of foam in the high permeability layer helps control the relative acid permeability, and acid can still penetrate the low permeability layer without resistance of foam.

Few studies have been reported of foam in fractures. Kovscek et al. [16] experimentally studied nitrogen, water and foam flow through a transparent rough-walled rock fracture with a hydraulic aperture of 30 μm. In these experiments, foam flow resistance was approximately 100–540 times greater than that of nitrogen for gas fractional flow ranging from 0.60–0.99.

Our purpose is to understand the mechanisms of foam flow in fractures and predict foam diversion in heterogeneous fracture systems. We derive below a theory to predict the foam apparent viscosity, starting from the existing theory for foam flow in capillary tubes. We made a uniform fracture model and conducted experiments to verify the theory. Also a heterogeneous fracture model was set up and used to study foam diversion. Finally, we developed a model to predict the sweep efficiency in multiple heterogeneous fractures with log-normal distributed apertures.

2. Theory

2.1. Apparent viscosity

Gas has a very low viscosity compared with oil and water. However, when gas is a dispersed phase, as in foam, its apparent viscosity is greatly increased, i.e., its mobility is greatly reduced. Hirasaki and Lawson [17] described a mathematical model for apparent viscosity in a smooth capillary tube for bubbles large enough that they travel sequentially along the tube. They found that the most important variable affecting foam apparent viscosity in uniform, smooth capillaries is foam texture or bubble size, which determines the number of interfaces per unit length. Dynamic changes at these interfaces strongly influence apparent viscosity, which is the sum of three contributions as in Fig. 1:

(1) Slugs of liquid between gas bubbles resist flow.
(2) Viscous and capillary forces result in interface deformation against the restoring force of surface tension. The different curvatures at the front and rear of a moving bubble dictate the pressure drop required for bubble motion.
(3) The surfactant is swept to accumulate at the back and be depleted at the front of the bubble, which causes a surface tension gradient that resists flow.

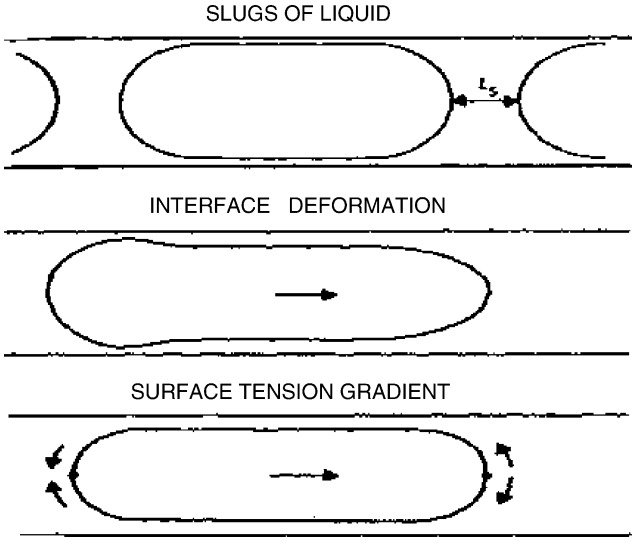

Fig. 1. Mechanisms affecting apparent viscosity in smooth capillaries (Hirasaki and Lawson, 1985).

The goal of our research is to find the optimum condition to divert the greatest amount of surfactant solution into thinner fracture regions. For that purpose, we first adapt the above model for capillary tubes to the case of a uniform fracture and describe experiments to confirm the validity of the model and determine the parameters involved. Then we extend both model and experiments to parallel flow in fractures of different thickness.

As indicated above, there are three contributions to the apparent viscosity of foam in a circular smooth capillary tube. The first is that from liquid between the bubbles, which is given by Eq. (1). This equation is also applicable to flow in a fracture of uniform thickness that is less than the bubble diameter.

$$\mu_{\text{app}}^{\text{liq}} = (1 - f_{\text{g}})\mu^{\text{liq}} \tag{1}$$

where μ^{liq} is the viscosity of pure liquid and f_{g} is the gas fractional flow.

The contribution of deformation of the foam bubbles to apparent viscosity in a uniform fracture can be predicted by comparing with that from foam flow in a capillary tube. From Hirasaki and Lawson [17], the equation for the net dynamic pressure drop across a single bubble is:

$$\Delta p_{\text{dynamic}} = 2.26 \left(\frac{\sigma}{r_{\text{c}}}\right) \left(\frac{3\mu^{\text{liq}} U}{\sigma}\right)^{2/3} \left[\left(\frac{r_{\text{c}}}{R}\right)^2 + 1\right] \tag{2}$$

Here U is the velocity of the bubble, σ is the surface tension, r_{c} is the radius of curvature of gas–liquid interface and R is the capillary radius. When the bubbles are not in contact $r_{\text{c}} = R$ and this equation simplifies to Bretherton's result [18]. For flow of large bubbles between parallel plates, a similar equation applies but without the term in brackets as above because the radius of the bubble as seen from above, which is the second and larger radius of curvature of the bubble periphery, is much greater than r_{c}:

$$\Delta p_{\text{dynamic}} = 2.26 \left(\frac{\sigma}{r_{\text{c}}}\right) \left(\frac{3\mu^{\text{liq}} U}{\sigma}\right)^{2/3} \tag{3}$$

The apparent viscosity from the contribution of foam bubble deformation in a uniform fracture can be predicted from the equations for plane-Poiseuille flow:

$$\mu_{\text{app}}^{\text{shape}} = \frac{n_{\text{L}} \Delta p_{\text{dynamic}} b^2}{12U} = \frac{0.57\mu^{\text{liq}}(n_{\text{L}} b)(3\mu^{\text{liq}} U/\sigma)^{-1/3}}{r_{\text{c}}/b} \tag{4}$$

where n_{L}, the number of equivalent lamellae per unit length, is a function of the number of bubbles per unit area and b is the fracture aperture or the distance between the two parallel plates. If the bubbles are distributed uniformly, from the derivation in

Appendix A, one finds

$$n_L = \left[\frac{3 f_g b}{4\pi r_B^3}\right]^{1/2} \tag{5}$$

where f_g is the gas fractional flow and r_B is the equivalent bubble radius. The equivalent bubble diameter is assumed to be larger than the aperture. If the bubbles are not in contact, the radius of curvature, r_c, is equal to the half aperture of the fracture, and substitution of Eq. (5) into Eq. (4) yields

$$\frac{\mu_{app}^{shape}}{\mu^{liq}} = 0.56\left(\frac{3\mu^{liq}U}{\sigma}\right)^{-1/3} f_g^{1/2}\left(\frac{b}{r_B}\right)^{3/2} \quad \text{where}$$

$$\frac{b}{2r_B} \le 1 \tag{6}$$

The total apparent viscosity can be obtained from measuring the pressure difference across the model. That is, from plane-Poiseuille equations:

$$\mu_{app} = \frac{b^2|\nabla p|}{12U} \tag{7}$$

where $|\nabla p|$ is the pressure gradient.

By comparing the sum of μ_{app}^{shape} and μ_{app}^{liq} with the value of μ_{app}, the contribution from surface tension gradient was found to be insignificant in our system, as discussed further below.

2.2. Foam diversion

Consider flow into two fractures of different thickness. The velocities in both fractures need to be determined to get the apparent viscosity either by theory or measurement. If only water or surfactant solution is flowing and if the pressure gradient is the same in the two regions, the velocity ratio can be obtained from Eq. (8):

$$\frac{U_1}{U_2} = \left(\frac{b_1}{b_2}\right)^2 \tag{8}$$

The velocity ratio can be found for foam flow. If the contribution to apparent viscosity from bubble deformation dominates, combining Eqs. (6) and (7) yields Eq. (9).

$$b^{-1/2}U^{2/3} = 0.21(\mu^{liq})^{-2/3} f_g^{-1/2} r_B^{3/2} \sigma^{-1/3} |\nabla p| \tag{9}$$

If it is further assumed that gas fractional flow and the pressure gradient are the same in both regions, the right side of this equation is the same for both regions. Thus, the ratio of Eq. (9) for the two regions gives

$$\frac{U_1}{U_2} = \left(\frac{b_1}{b_2}\right)^{3/4} \tag{10}$$

Then from overall material balance, the velocities in both fractures can be estimated. Moreover, taking the ratio of Eq. (6) for the two regions and eliminating the velocity ratio with Eq. (10), one finds that the apparent viscosity from the deformation contribution is proportional to 5/4 power of aperture as in Eq. (11). This result shows the possibility of foam diversion into the thinner fracture because of the higher resistance to flow in the thicker fracture.

$$\frac{\mu_{app,1}}{\mu_{app,2}} = \left(\frac{b_1}{b_2}\right)^{5/4} \tag{11}$$

2.3. Bulk foam in fractures

Princen [19] modeled the theory for rheology of foams and highly concentrated emulsions. Hirasaki and Lawson [17] developed the model to describe bulk foam apparent viscosity in a capillary tube. But the theory can be applied only to bubbles with the shape of pentagonal dodecahedra, which are obtained only at quite high gas fractional flow, where all the bubbles in the system are closely-packed.

Many semi-empirical expressions are available for describing the shear viscosity of concentrated dispersions of hard spheres. The most widely used is the functional form suggested by Krieger and Dougherty [20].

$$\eta_r = (1 - K\phi)^{-2.5/K} \tag{12}$$

where η_r is the relative viscosity, which is the ratio of the viscosity of emulsion to the viscosity of water. ϕ is the volume fraction of emulsion in water. K is the crowding factor and equal to the reciprocal of the dense random packing limit volume fraction ϕ_{max}, at which η_r diverges to infinity. For random close packing of monodisperse hard spheres, they found $\phi_{max} = 0.64$ and $K = 1.56$.

Mooney [21] developed another expression for the relative viscosity of emulsions where the particles behave as rigid spheres.

$$\eta_r = \exp\left[\frac{2.5\phi}{1 - K\phi}\right] \tag{13}$$

The crowding factor K in the above two equations can be smaller when the particles are not uniformly distributed in size or are deformable as in foams because these factors can cause an increase of the dense random packing limit volume fraction.

Pal [22] studied the rheology of polymer-thickened emulsions and found that the increase of the viscosity ratio of continuous phase to dispersed phase enhances the internal circulation effect, which leads to a decrease in the relative viscosity. He suggested the following equation.

$$\eta_r^{1/K_I} = \exp\left[\frac{2.5\phi}{1 - K\phi}\right] \tag{14}$$

where K_I is a factor which takes into account internal circulation effects and is given by

$$K_I = \left[\frac{1 + 0.4(\eta_c/\eta_d)}{1 + (\eta_c/\eta_d)}\right] \tag{15}$$

In the above equation, η_c is the viscosity of the continuous phase and η_d is the viscosity of the dispersed phase. Pal [22] also suggested a crowding factor $K = 1.04$, which means the dense random packing limit volume fraction $\phi_{max} = 0.96$. Predictions of these three models are compared with our data in Section 4.4.

2.4. Prediction of sweep efficiency in heterogeneous fractures

By using a similar method to that described by Lake [23], we developed a mathematical model to describe foam flooding in parallel, heterogeneous fractures with different apertures. We assumed no crossflow between fractures, the same pressure drop across each fracture, plug flow in each region and foam apparent viscosity determined by the velocity of foam flow at steady state, i.e., the velocity after all layers have been swept.

First, we apply this model in heterogeneous fractures with two regions of different apertures. We assume that foam completely displaces the water initially present in each region as it advances. Suppose $b_1 > b_2$. Then integration of the equation to the time when $x_1 = 1$ yields

$$x_2 = \frac{\{[M_2^2 + k_2\mu_{\text{app},1}(1 - M_2)(1 + M_1)/(k_1\mu_{\text{app},2})]^{1/2} - M_2\}}{1 - M_2} \tag{16}$$

where M_1 and M_2 are the mobility ratios between foam and water in the two fractures. (See Appendix B for derivation of the equations in this section and definitions of some parameters.)

The dimensionless time in injected liquid pore volumes when this occurs is

$$\text{Dimensionless time} = \frac{(x_2 b_2 + b_1)(1 - f_g)}{b_1 + b_2} \tag{17}$$

From this time until that when $x_2 = 1$ for the thinner fracture, v_1 in the thicker fracture is given by Eq. (B.1) with $x_1 = 1$.

Then similarly we can get the dimensionless time in injected liquid pore volumes when $x_2 = 1$:

$$\text{Dimensionless time} = \frac{(z_1 b_1 + b_2)(1 - f_g)}{b_2 + b_1} \tag{18}$$

where z_1 exceeds 1 by the dimensionless length of a region of thickness b_1 needed to hold the foam produced from fracture 1 up to that time.

$$z_1 = 1 + \frac{k_1\mu_{\text{app},2}}{k_2\mu_{\text{app},1}}\left[\frac{(1 + M_2)}{2} - \frac{(1 + M_1)k_2\mu_{\text{app},1}}{2k_1\mu_{\text{app},2}}\right] \tag{19}$$

2.5. Fractures with log-normal distribution apertures

Normally there are more than two fractures. For multiple fractures, the key is to get the number of fractures that have been swept at some FWR, the ratio of foam to water being produced. The number N of fractures where foam has broken through at some FWR is given by

$$\text{FWR} = \frac{\sum_{i=1}^{N} Q_i}{\sum_{i=N+1}^{N_L} Q_i} \tag{20}$$

where Q_i is the flow rate in the ith fracture and N_L is the total number of fractures. Then by a derivation similar to that above and in Appendix B for the two heterogeneous fractures, the sweep efficiency and the dimensionless time can be obtained. The sweep efficiency is the percentage of the overall fracture volume that contains foam. The dimensionless time is the injected liquid pore volumes of foam injected.

$$\text{Sweep efficiency} = \frac{\sum_{i=1}^{N} b_i + \sum_{i=N+1}^{N_L} x_i b_i}{\sum_{i=1}^{N_L} b_i} \tag{21}$$

$$\text{Dimensionless time} = \left(\frac{\sum_{i=1}^{N_L} z_i b_i}{\sum_{i=1}^{N_L} b_i}\right)(1 - f_g) \tag{22}$$

where f_g is the gas fractional flow.

Many researchers [24–27] have found that the fracture aperture distribution of reservoirs is approximately log-normal. Such a log-normal aperture distribution can be described by the function

$$C = \frac{1 + \text{erf}(\tau/\sqrt{2})}{2} \tag{23}$$

where

$$\tau = \frac{\ln(b/\bar{b})}{\sqrt{V}}$$

The function $C(b)$ is the fraction of the samples that have aperture less than b, i.e., the cumulative probability function. The parameter $\bar{b}$ is the median or log-mean aperture. The parameter V is the variance of the distribution. If the log-mean value $\bar{b}$ and variance V are known, different values of b can be obtained and used in Eqs. (21) and (22) to get the sweep efficiency and dimensionless time.

3. Experimental methods

The fracture model used is shown in Figs. 2 and 3. It consists mainly of two parallel glass plates. Changing the gasket thickness between the plates can change the aperture of the fracture. The thick glass is from Lone Star Glass Company, Houston, TX. It is borosilicate glass with 35.56 cm length and 20.32 cm width. Its thickness is 6.35 ± 0.3 mm. The surface of the glass is polished. The thin glass is Schott D-263 borosilicate glass from Precision Glass & Optics Company, Santa Ana, CA. It is 25.4 cm long and 7.62 cm wide. It is 0.10 ± 0.01 mm thick. It is not quite long enough to span the flow area. For experiments

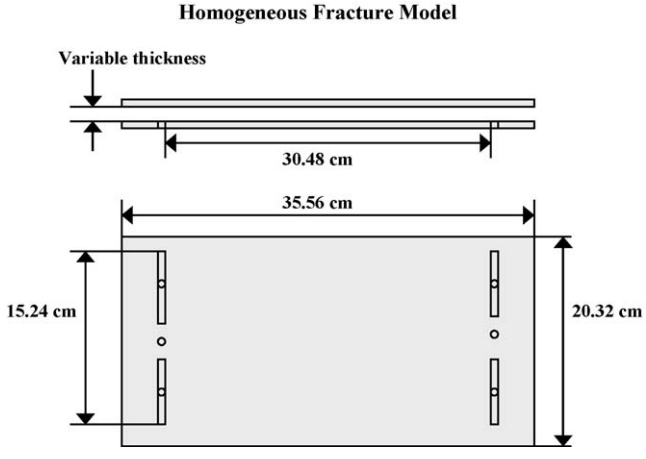

Fig. 2. Detailed diagram of homogeneous fracture model.

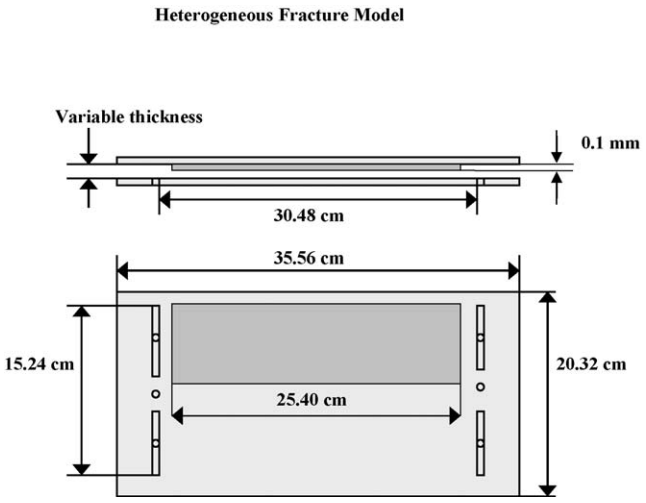

Fig. 3. Detailed diagram of heterogeneous fracture model.

with a homogeneous fracture, the uniformly thick gasket keeps a uniform distance between the plates. The procedure for making the heterogeneous fracture is: (1) adhere the thin glass plate described above to half of one of the thick glass plates by Norland optical adhesive; (2) roll the thin glass on the thick glass to remove any air and excess adhesive between them; (3) cure the adhesive by a high intensity ultraviolet lamp (Model Spectroline SB-100P) for over 48 h.

A schematic diagram of the equipment for the foam experiments is shown in Fig. 4. A Harvard syringe infusion pump (Model 22) is used to inject surfactant solution and a Matheson mass flow controller (Model 8270) is used to inject air into the foam generator. Relatively uniform bubbles can be generated only when the air and liquid are introduced on opposite sides of the frit in the foam generator. Choosing frits with different pore sizes can generate different sizes of bubbles. The borosilicate frits are from Chemglass Company, Vineland, NJ. Two grooves were made along the inlet and outlet of the fracture model to assure uniform pressures at both locations.

The surfactant solution in the experiments was 0.5% C13-4PO and 0.5% STEOL CS330. C13-4PO is from Harcros Company, and its chemical description is propoxylated iso-C13 alcohol ether sulfate, ammonium salt. STEOL CS330 is from

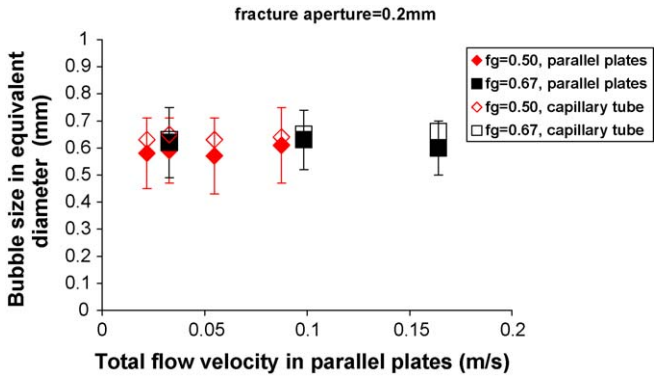

Fig. 5. Bubble size distribution, error bars show the standard deviation from bubble size measurement.

Stepan Company and its chemical description is C12-3EO sulfate. The solution contained 0.23% NaCl, 0.07% $CaCl_2$ and 0.04% $MgCl_2$. The bubble diameters in the experiments ranged from 0.04–1.0 mm. The aperture was 0.1, 0.2 and 0.3 mm for homogeneous fracture experiments and the combinations of 0.1 mm/0.2 mm or 0.05 mm/0.15 mm for heterogeneous fracture experiments. The gas fractional flow range was from 0.0–0.9. The values used for the viscosity of solution and surface tension were 1 mPa s and 28 mN/m, respectively.

4. Results and discussion

4.1. Bubble size measurement

Two different methods were used to determine the average bubble size: image analysis and capillary tube experiments. From analysis of images taken just after foam flow has stopped, the average bubble size and bubble size distribution can be obtained with the help of image analysis software "IPTK", which was developed by Reindeer Graphics Inc., Asheville, NC. The average bubble size may also be obtained by counting the number of lamellae in a given capillary tube length by letting foam flow into capillary tubes with diameters less than the bubble diameter. The mean bubble sizes obtained from image analysis and capillary tube experiments are in good agreement as shown in Fig. 5. The bubble size shown is the equivalent spherical

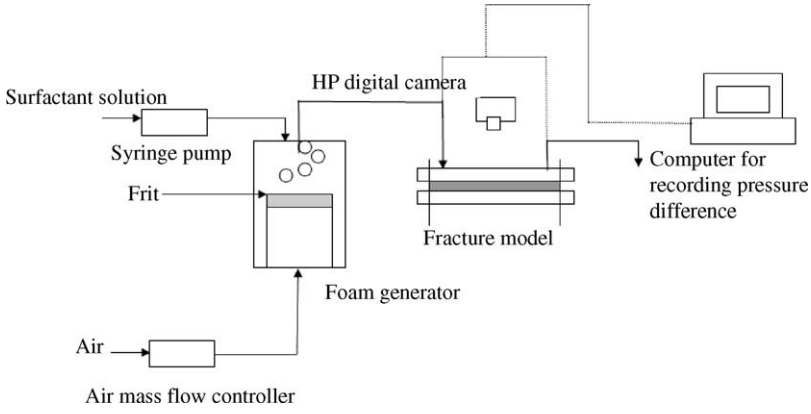

Fig. 4. Set–up diagram for foam mobility control experiment in fracture model.

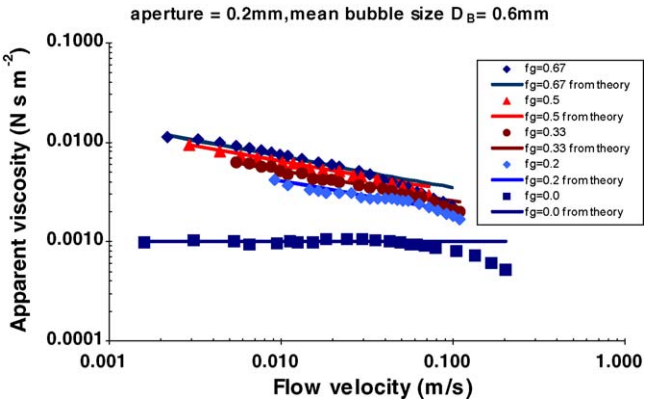

Fig. 6. Effect of flow rate and fractional flow on apparent viscosity.

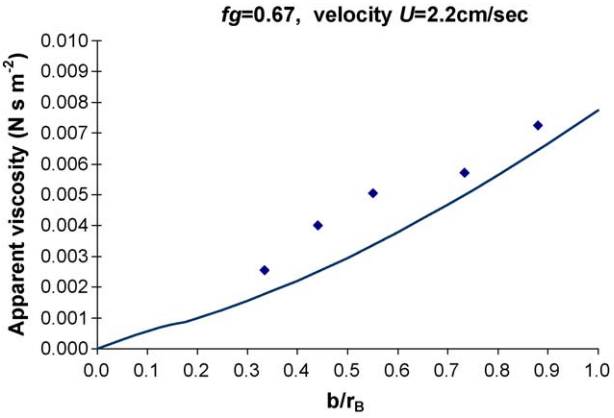

Fig. 7. Effect of ratio of aperture/bubble size on apparent viscosity.

diameter. The standard deviation of the bubble size distribution is about 20%. From Fig. 5, the mean bubble size and standard deviation remain constant at different flow rates and different gas fractional flow. Other experiments showed similar behavior as long as the bubble equivalent diameter was less than five times the aperture.

4.2. Apparent viscosity in homogeneous fractures

Experiments were conducted to investigate the effects of flow rate, bubble size, gas fractional flow, and aperture on the apparent viscosity of foam flowing in uniform fractures. From the experiments, the most important variable affecting foam viscosity in a homogeneous fracture system is foam texture. Foam of finer texture has more lamellae per unit length and, as a result, greater resistance to flow. The foam bubbles in our experiments are individual bubbles because the aperture is smaller than the equivalent diameter of the bubbles. No aggregation or coalescence of bubbles was observed in cases for which data are reported.

Results for a homogeneous fracture with an aperture of 0.2 mm are shown in Fig. 6. The data fit the theory (based on contributions from liquid and bubble deformation without the contribution from the surface tension gradient) quite well at low flow rates. The apparent minimal contribution from surface tension gradient likely is due to the surfactant concentration being well above the CMC and to the presence of inorganic electrolyte, which reduces electrostatic repulsion between surfactant ions at the surface and those in the liquid phase near the surface. As a result, adsorption and desorption should be rapid and surface tension gradient small. Because the theory is based on Hele-Shaw flow, which is valid for creeping flow, the data begin to deviate from the theory when the Reynolds number exceeds about 1–10, depending on bubble size and gas fractional flow. Here the Reynolds number is defined as

$$Re = \frac{\rho^{\mathrm{liq}} b U}{\mu^{\mathrm{liq}}} \tag{24}$$

where ρ^{liq} is the density of the liquid. At the velocity $U = 0.1$ m/s, the Reynolds number Re is about 10. As Fig. 6 shows, the bubbles produce a shear thinning effect.

Fig. 6 also shows the effect of gas fractional flow f_g on apparent viscosity. With the increase of f_g or foam quality, the number of lamellae per unit length or number of bubbles per unit area increases, which causes apparent viscosity to increase in proportion to $f_g^{1/2}$, as in Eq. (6). For $f_g = 0.9$, individual bubbles remained circular as seen from above, i.e., deformation was minimal. However, data for $f_g = 0.9$ are not plotted because only a few reliable data points could be obtained at the low liquid flow rates involved. No data are given for larger f_g because significant coalescence was observed.

Fig. 7 shows the effect of the ratio of aperture b to bubble size r_B on apparent viscosity. The number of lamellae per unit length or of bubbles per unit area increases with decrease of bubble size and increase of aperture at fixed fractional flow. Accordingly, Eq. (6) shows that the contribution to apparent viscosity from bubble deformation is proportional to the 3/2 power of this ratio. As a result, apparent viscosity would be significantly higher than in Fig. 7 for smaller bubbles only slightly greater than aperture thickness, i.e. $\frac{b}{r_B}$ approaches 2. On the other hand, the apparent viscosity is larger for large apertures. This feature is important in foam application, because it indicates that foam of the same bubble size and gas fractional flow can reduce fluid flow in high permeability regions and divert flow into low permeability regions.

4.3. Apparent viscosity and sweep in heterogeneous fractures

Experiments with the heterogeneous fracture model were performed for average bubble diameters of 0.4 and 0.6 mm, which are larger than the thicker aperture to meet the conditions of our theory. The Reynolds numbers were 0.22 and 0.44. Two different aperture ratios were used in the experiments, 1:2 and 1:3.

4.3.1. Apparent viscosity

The apparent viscosity in each region can be calculated from Eq. (7), using the pressure difference obtained in experiments. We assume that gas fractional flow is the same in thinner and thicker apertures and that velocity in each layer can be obtained from Eq. (10) and material balance, as indicated above. Also the apparent viscosity can be estimated from the sum of Eqs. (6) and (1). We consider first the case in which both regions of

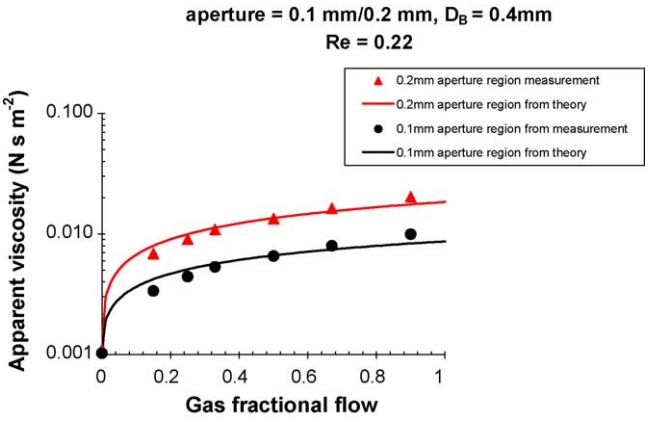

Fig. 8. Apparent viscosity for aperture ratio of 0.1 mm/0.2 mm, bubble size = 0.4 mm and $Re = 0.22$.

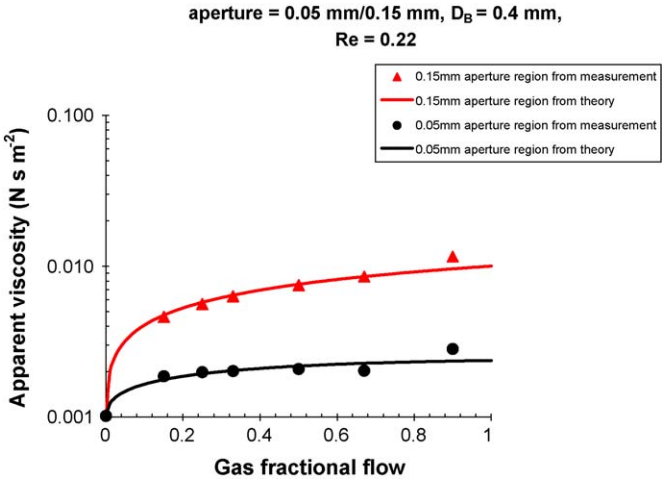

Fig. 9. Apparent viscosity for aperture ratio of 0.05 mm/0.15 mm, bubble size = 0.4 mm and $Re = 0.22$.

the fracture are fully filled with foam, so that there are minimal lateral pressure gradients and cross flow. The theoretical and experimental results are compared in Figs. 8 and 9. For the range of experimental conditions listed at low Reynolds' number (less than 1) the apparent viscosity from measurement of pressure difference agrees well with that from theory prediction. This confirms that the assumption of equal gas fractional flow is valid.

From Figs. 8 and 9, we can see the effects of the aperture ratio on the magnitude of diversion in heterogeneous fractures. The diversion depends on the apparent viscosity difference between the two regions. If we ignore the contribution of liquid slug to the total apparent viscosity, Eq. (11) predicts that the apparent viscosity is proportional to the 5/4 power of aperture thickness. So the apparent viscosity ratio is largest in Fig. 9, which is with 3:1 aperture ratio.

4.3.2. Sweep efficiency

Photographs were taken during experiments to investigate the sweep by foam and surfactant solution in heterogeneous fractures. An example of foam/surfactant solution sweep is shown in Fig. 11. For comparison, the picture of sweep by surfactant solution alone is shown in Fig. 10. We use "pore volume" (PV) to normalize the amount of foam or liquid injected. "Total pore volume" (TPV) is defined as the total volume of liquid and gas injected divided by the space in fractures. "Injected liquid pore volume" LPV is the volume of liquid divided by the space in fractures. The relationship between total pore volume and injected liquid pore volume is shown in Eq. (25).

$$\mathrm{LPV} = \mathrm{TPV}(1 - f_g) \tag{25}$$

The injection of foam bubbles together with surfactant solution greatly improves the sweep over the injection of surfactant solution only. From Fig. 10 for 0.05 mm/0.15 mm fracture, at Reynolds number 0.22, it takes about 6.6 pore volumes of surfactant solution to sweep the 0.05 mm aperture region, while theory predicts that 7.0 pore volumes are needed. With gas fractional flow 0.9 and bubble size 0.4 mm in diameter, only 0.15 injected liquid pore volume of surfactant solution is needed, as shown in Fig. 11. The amount of surfactant solution needed to

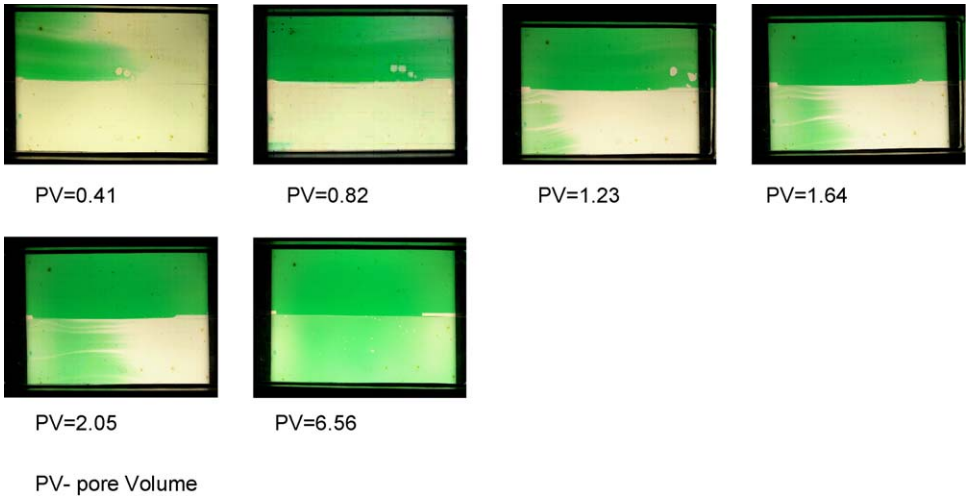

Fig. 10. Surfactant solution sweeping heterogeneous fracture, $Re = 0.22$, fracture aperture ratio = 0.05 mm (bottom)/0.15 mm (top). PV refers to pore volume of the entire heterogeneous fracture.

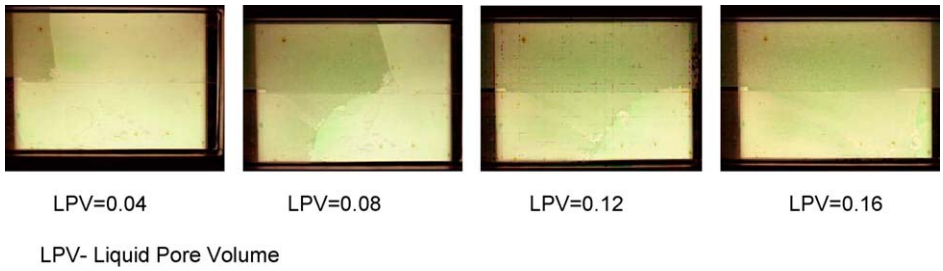

Fig. 11. Foam/surfactant solution sweeping heterogeneous fracture, $Re = 0.22$, $f_g = 0.9$, fracture aperture ratio = 0.05 mm (bottom)/0.15 mm (top), $D_B = 0.4$ mm (note: LPV is the injected liquid pore volumes).

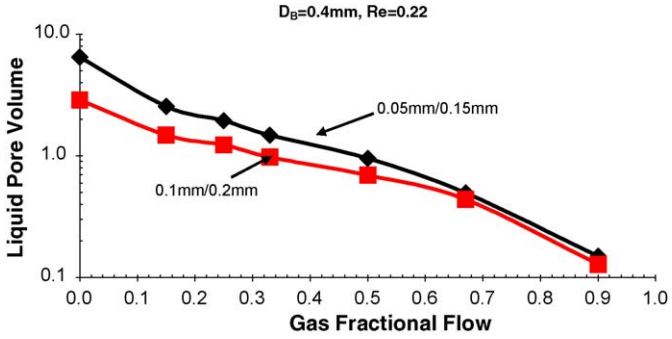

Fig. 12. Liquid pore volumes of surfactant introduced when foam completely sweeps the given fracture at different fracture aperture ratios.

sweep both regions is reduced by a factor of more than 40. This large difference is partly the result of the higher apparent viscosity in the thicker region and partly because less liquid is required to fill a given volume when foam is used.

Experiments were also conducted for other gas fractional flows with aperture ratios of 2 and 3. The results are shown in Fig. 12. It is easily seen that high gas fractional flow can give better sweep efficiency, i.e., reduction in the amount of surfactant solution required to sweep both portions of the heterogeneous fracture. As might be expected, more surfactant solution is required for the higher aperture ratio.

Fig. 13 shows the comparison between the theoretical predictions and experimental results for foam/surfactant sweep in a heterogeneous fracture with 1:3 aperture ratio. Agreement is good. This validates the assumption of minimal crossflow. It also indicates that the assumption of equal gas fractional flow in different layers is reasonable for these conditions.

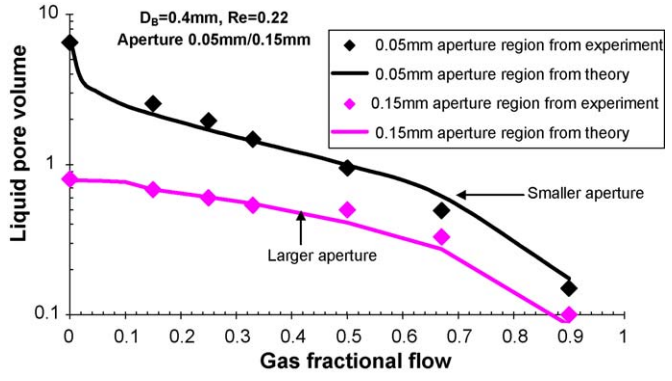

Fig. 13. Comparison between the calculation and the experimental results of the liquid pore volumes of surfactant needed for foam/surfactant sweep in heterogeneous fractures with 1:3 aperture ratio.

4.4. Bulk foam apparent viscosity

The apparent viscosity for bulk foam flow in fractures was measured at different aperture, flow velocity and bubble size as shown in Fig. 14. The highest gas fractional flow is 0.67 because we found that bubbles began to coalesce for gas fractional flows exceeding 0.67.

The predictions from Krieger and Dougherty equation, Mooney equation and Pal's model are also plotted in Fig. 14. For the first two equations ϕ_{max} has been increased to 0.99 and K decreased to 1.01 because we deal with deformable bubbles, not hard spheres. Even with this change there are still significant deviations between the predictions and experimental results although agreement is much better than with the corresponding hard sphere values given above. In contrast, the experimental measurements match well the prediction of Pal's model.

Because the viscosity of water is much larger than that of gas, K_I is close to 0.4. We still use 0.96 as the dense random packing limit volume fraction. Then the crowding factor K is 1.04. Because the viscosity of the dispersed phase is small in the foam case, the velocity gradient near the bubble interfaces is smaller than for solid particles, yielding a lower apparent viscosity.

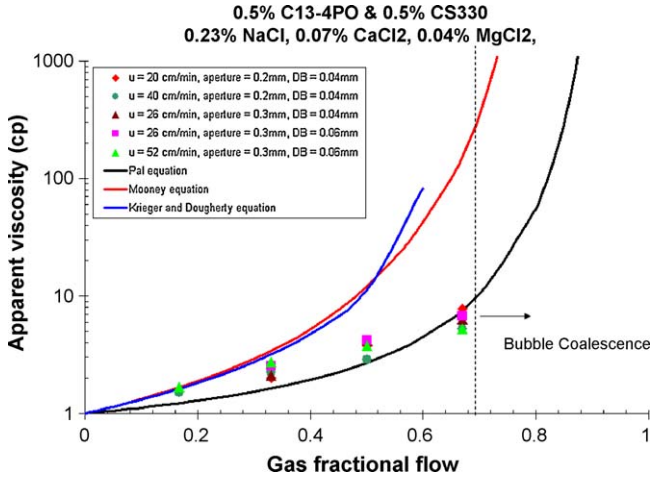

Fig. 14. Bulk foam apparent viscosity in fractures, measurement and prediction.

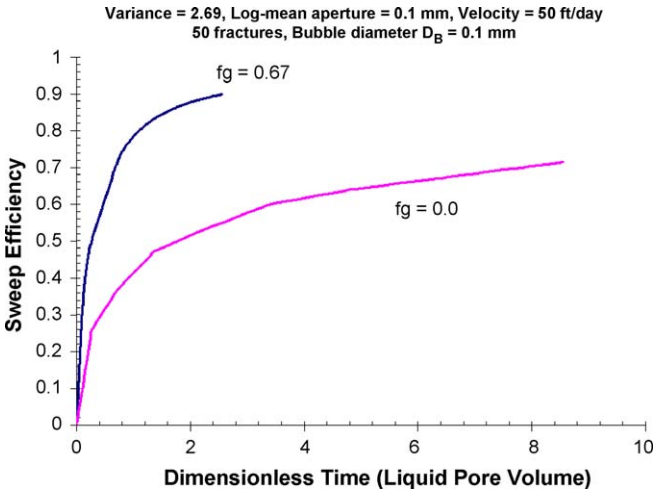

Fig. 15. Calculation results of the foam/water sweep in heterogeneous fracture with log-normal distribution of apertures for bubble diameter 0.1 mm.

4.5. Prediction of sweep efficiency in heterogeneous fractures with a log-normal distribution of apertures

Calculations for the sweep efficiency in a heterogeneous fracture system with a log-normal distribution of apertures were performed, and the results are shown in Fig. 15. The variance V is set to be 2.69 and the log-mean aperture is 0.1 mm.

This fracture model has 50 layers, and the bubble diameter is 0.1 mm. At velocity 50 ft/day (1.06 cm/min), the sweep efficiency can be almost 90% for gas fractional flow at 0.67 with two injected liquid pore volume, which is a big improvement over water flood at gas fractional flow $f_g = 0$. In this calculation, when the aperture is larger than the bubble diameter, the bubbles are considered as bulk foam.

With higher apparent viscosity, we can get more improvement in sweep efficiency by foam flooding over water flooding. But there will be high pressure drop with high apparent viscosity. The optimum between pressure drop and sweep efficiency needs to be considered. At present we do not know how to predict bubble size in a fracture system.

5. Conclusions

For the experimental conditions described above, i.e., sufficiently low Reynolds numbers, gas fractional flow and bubble sizes where no coalescence or break-up occurs, the following conclusions apply for the foam flow through a smooth, uniform fracture:

(1) The foam texture (a measure of the bubble volume) is a key parameter in determining n_L, the number of lamellae per unit length, which is the main factor affecting the foam viscosity in smooth uniform fractures when the (undeformed) bubble diameter exceeds fracture aperture. Changes which increase n_L, e.g., higher gas fractional flow f_g and larger ratios of aperture thickness to bubble size, cause apparent viscosity to increase. The aperture thickness effect is the basis for producing a more uniform sweep by the use of foam.
(2) The apparent viscosity is the sum of two contributions: that resulting from liquid between bubbles and that resulting from the resistance to deforming the interface when a bubble passes through a fracture. The surface tension gradient contribution does not appear to be significant in our experiments.
(3) Pal's equation can well predict the apparent viscosity of bulk foam in fractures, i.e., when bubble diameter is somewhat less than fracture aperture.

We investigated different factors' effects on sweep efficiency by foam in smooth heterogeneous fractures and applied our theory to this situation assuming the same f_g in each portion of the fracture and no crossflow. Some conclusions can be made accordingly.

(1) Foam apparent viscosity in each portion of a heterogeneous fracture can be calculated using the theoretical result for a homogeneous fracture.
(2) Foam can greatly improve the sweep efficiency in a heterogeneous fracture system. The amount of surfactant solution required is reduced substantially both by foam's ability to divert flow into smaller fractures and by the need for less liquid to fill a given volume of fractures.
(3) Gas fractional flow, aperture ratio and bubble size can greatly affect the sweep efficiency.
(4) Agreement of theoretical predictions and experimental results confirms validity of the theory's assumptions of equal f_g, minimal crossflow and constant bubble size.

Acknowledgements

The authors acknowledge Maura Puerto and Dick Chronister for their assistance. The financial support of the U.S. DOE Award #DE-FC26-03NT15406 is gratefully acknowledged.

Appendix A. Derivation for the equivalent lamellae per unit length n_L

Assuming that bubbles are distributed uniformly, the total number of bubbles N_{bubble} in a rectangular area having length L and width W is:

$$N_{bubble} = (n_L L) \times (n_L W) = L W n_L^2 \tag{A.1}$$

Then the total volume occupied by gas is:

$$v_{gas} = N_{bubble} \left(\frac{4}{3}\right) \pi r_B^3 = \left(\frac{4}{3}\right) \pi r_B^3 L W n_L^2 \tag{A.2}$$

However, the total volume occupied by gas is also given by:

$$v_{gas} = L W b f_g \tag{A.3}$$

where b is the fracture thickness.

Combine the above two equations to obtain the number of equivalent lamellae per unit length:

$$n_{\mathrm{L}} = \left[\frac{3 f_{\mathrm{g}} b}{4\pi r_{\mathrm{B}}^3}\right]^{1/2} \tag{A.4}$$

Appendix B. Calculation for the sweep efficiency in two layer heterogeneous fractures

Based on the assumptions listed at the beginning of Section 2.3, the calculation for the sweep efficiency in two layer heterogeneous fractures was derived as below.

The foam front position in each region may be determined from Darcy's law

$$\frac{\mathrm{d}x_l}{\mathrm{d}t} = v_l = \frac{-k_l \lambda_{\mathrm{re}l} \Delta p}{L}, \quad l = 1, 2 \tag{B.1}$$

where v_l is the velocity in region l, and $\lambda_{\mathrm{re}l}$ is the relative mobility in region l defined by

$$\lambda_{\mathrm{re}l} = \left[\frac{x_l}{\lambda_{\mathrm{app},l}} + \frac{1 - x_l}{\lambda^0}\right]^{-1}$$

$$= [\mu_{\mathrm{app},l} x_l + \mu^0 (1 - x_l)]^{-1} \quad \text{for } x_l < 1 \tag{B.2}$$

or

$$\lambda_{\mathrm{re}l} = \lambda_{\mathrm{app},l} = \mu_{\mathrm{app},l}^{-1} x_l \quad \text{for } x_l > 1$$

where $\lambda_{\mathrm{app},l}$ is the relative mobility of foam, λ^0 is the relative mobility of water, $\mu_{\mathrm{app},l}$ is the apparent viscosity of foam in region l and μ^0 is the water viscosity.

Taking the ratio of the velocities in the two regions will eliminate time and the pressure drop since both regions experience the same Δp. Thus, before breakthrough ($x_l < 1$), we have

$$\frac{\mathrm{d}x_1}{\mathrm{d}x_2} = \left(\frac{k_1}{k_2}\right)\left(\frac{\mu_{\mathrm{app},2}}{\mu_{\mathrm{app},1}}\right)\frac{[x_2 + (1 - x_2)M_2]}{[x_1 + (1 - x_1)M_1]} \tag{B.3}$$

where M_1, M_2 are the mobility ratios, e.g. $M_l = \lambda_{\mathrm{app},l}/\lambda^0 = \mu^0/\mu_{\mathrm{app},l}$, k_1, k_2 are the permeabilities, $k_l = b_l^2/12$ in fractures where b_l is the aperture. Moreover,

$$\int_0^{x_1} k_2 \mu_{\mathrm{app},1}[x_1 + (1 - x_1)M_1]\mathrm{d}x_1$$

$$= \int_0^{x_2} k_1 \mu_{\mathrm{app},2}[x_2 + (1 - x_2)M_2]\mathrm{d}x_2 \tag{B.4}$$

$$\frac{(1 - M_1)x_1^2}{2} + M_1 x_1 = \frac{k_1 \mu_{\mathrm{app},2}}{k_2 \mu_{\mathrm{app},1}}\left[\frac{(1 - M_2)x_2^2}{2} + M_2 x_2\right] \tag{B.5}$$

When the foam front reaches the outlet of the thicker region ($x_1 = 1.0$), the dimensionless front position at the thinner region is

$$x_2 = \frac{\{[M_2^2 + (1 - M_2)(1 + M_1)(k_2 \mu_{\mathrm{app},1})/(k_1 \mu_{\mathrm{app},2})]^{1/2} - M_2\}}{1 - M_2} \tag{B.6}$$

Then the dimensionless time in the injected liquid pore volume needed for the sweep of thicker region is

$$\text{Dimensionless time} = \frac{(x_2 b_2 + b_1)(1 - f_{\mathrm{g}})}{b_1 + b_2} \tag{B.7}$$

As the thinner region continues to be swept, the hypothetical dimensionless front position z_1 in the thicker region (outside the fracture) can be obtained from

$$\frac{\mathrm{d}z_1}{\mathrm{d}x_2} = \left(\frac{k_1}{k_2}\right)\left(\frac{\mu_{\mathrm{app},2}}{\mu_{\mathrm{app},1}}\right)[x_2 + (1 - x_2)M_2] \tag{B.8}$$

That is, the product $(z_1 - 1)lbw$ is the volume of foam produced from fracture 1 after foam breakthrough.

$$\int_1^{z_1} \mathrm{d}z_1 = \int_{x_2^0}^{x_2} \left(\frac{k_1}{k_2}\right)\left(\frac{\mu_{\mathrm{app},2}}{\mu_{\mathrm{app},1}}\right)[x_2 + (1 - x_2)M_2]\mathrm{d}x_2 \tag{B.9}$$

$$z_1 = 1 + \frac{k_1 \mu_{\mathrm{app},2}}{k_2 \mu_{\mathrm{app},1}}\left[\frac{(1 - M_2)(x_2^2 - (x_2^0)^2)}{2} + M_2(x_2 - x_2^0)\right] \tag{B.10}$$

Setting $x_2 = 1.0$, and $x_2^0 = \{[M_2^2 + (1 - M_2)(1 + M_1)(k_2 \mu_{\mathrm{app},1})/(k_1 \mu_{\mathrm{app},2})]^{1/2} - M_2\}/(1 - M_2)$, one finds

$$z_1 = 1 + \frac{k_1 \mu_{\mathrm{app},2}}{k_2 \mu_{\mathrm{app},1}}\left[\frac{(1 + M_2)}{2} - \frac{(1 + M_1)k_2 \mu_{\mathrm{app},1}}{2k_1 \mu_{\mathrm{app},2}}\right] \tag{B.11}$$

And the dimensionless time or the injected liquid pore volume needed to sweep the thinner region is

$$\text{Dimensionless time} = \frac{(z_1 b_1 + b_2)(1 - f_{\mathrm{g}})}{b_2 + b_1} \tag{B.12}$$

References

[1] A.R. Kovscek, C.J. Radke, Fundamentals of Foam Transport in Porous Media, in: L.L. Schramm (Ed.), Foams: Fundamentals and Applications in the Petroleum Industry, American Chemical Society, Washington DC, 1994, pp. 115–164.

[2] J.B. Lawson, J. Reisberg, Alternate Slugs of Gas and Dilute Surfactant for Mobility Control during Chemical Flooding, Society of Petroleum Engineers, 8839, Presented at SPE/DOE Enhanced Oil Recovery Symposium, Tulsa, OK, 1980, pp. 20–23.

[3] D. Wang, J. Cheng, Z. Yang, Q. Li, W. Wu, H. Yu, Successful Field Test of the First Ultra-Low Interfacial Tension Foam flood, Society of Petroleum Engineers, 72147, Presented at the SPE Asia Pacific Improved Oil Recovery Conference, Kuala Lumpur, Malaysia, 2001, pp. 8–9.

[4] G.J. Hirasaki, R.E. Jackson, M. Jin, J.B. Lawson, J. Londergan, H. Meinardus, C.A. Miller, G.A. Pope, R. Szafranski, D. Tanzil, Field demonstration of the surfactant/foam process for remediation of a heterogeneous aquifer contaminated with DNAPL, in: S. Fiorenza, C.A. Miller, C.L. Oubre, C.H. Ward (Eds.), NAPL Removal: Surfactants, Foams, and Microemulsions, Lewis Publishers, 2000.

[5] G.J. Hirasaki, D.L. Zhang, Surface chemistry of oil recovery from fractured, oil-wet, carbonate formations, Soc. Petroleum Eng. J. 9 (2) (2004) 151–162.

[6] J.F. Casteel, N.F. Djabbarah, Sweep improvement in CO_2 flooding by use of foaming agents, Soc. Petroleum Eng. Reservoir Eng. (1988) 1186–1192.

[7] F.M. Llave, F.T.-H. Chung, R.W. Louvier, D.A. Hudgins, Foams as Mobility Control Agents for Oil Recovery by Gas Displacement, Society of Petroleum Engineers/Department of Engineering, 20245, Prepared for Presentation at the SPE/DOE Seventh Symposium on EOR at Tulsa, OK, 1990, pp. 22–25.
[8] M. Zerhboub, K. Ben-Naceur, E. Touboul, R. Thomas, Matrix acidizing: a novel approach to foam diversion, Soc. Petroleum Eng. Production Facilities 9 (2) (1994) 121–126.
[9] H. Yaghoobi, J.S. Tsau, J.P. Heller, Improving CO_2 Floods in Heterogeneous Media, Society of Petroleum Engineers, 35403, Prepared for SPE/DOE Improved Oil Recovery Symposium at Tulsa, OK, 1996, pp. 21–24.
[10] S. Siddiqui, S. Talabani, S.T. Saleh, M.R. Islam, A Laboratory investigation of Foam Flow in Low Permeability Berea Sandstone Cores, Society of Petroleum Engineers, 37416, Prepared for Presentation at the 1997 SPE Production Operations Symposium at Oklahoma City, OK, 1997, pp. 9–11.
[11] H.J. Bertin, O.G. Apaydin, L.M. Castanier, A.R. Kovscek, Foam flow in heterogeneous porous media: effect of cross flow, Soc. Petroleum Eng. J. 4 (2) (1999) 75–82.
[12] W.T. Osterloh, M.J. Jante Jr., Effects of Gas and Liquid Velocity on Steady State Foam Flow at High Temperature, Society of Petroleum Engineers, 24179, Prepared for Presentation at the 1992 SPE/DOE Symposium on Enhanced Oil Recovery at Tulsa, OK, 1992, pp. 22–25.
[13] W.R. Rossen, M.W. Wang, Modeling foams for acid diversion, Society of Petroleum Engineers, 24179, Soc. Petroleum Eng. J. 6 (4) (1999) 92–100.
[14] L. Cheng, A.B. Reme, D. Shan, D.A. Coombe, W.R. Rossen, Simulating Foam Processes at High and Low Foam Qualities, Society of Petroleum Engineers, 59287, Presented at the SPE/DOE Improved Oil Recovery Symposium at Tulsa, OK, 2000, pp. 3–5.
[15] Q.P. Nguyen, P.K. Currie, P.K.J. Zitha, Effect of Capillary Cross-Flow on Foam-Induced Diversion in Layered Formations, Society of Petroleum Engineers, 82270, Presented at the SPE European Formation Damage Conference at Hague, Netherlands, 2003, pp. 13–14.
[16] A.R. Kovscek, D.C. Tretheway, P. Persoff, C.J. Radke, Foam flow through a transparent rough-walled rock fracture, J. Petroleum Sci. Eng. 13 (1995) 75–86.
[17] G.J. Hirasaki, J.B. Lawson, Mechanisms of foam flow in porous media: apparent viscosity in smooth capillaries, Soc. Petroleum Eng. J. 25 (2) (1985) 176–190.
[18] F.P. Bretherton, The motion of long bubbles in tubes, J. Fluid Mechanics 10 (1961) 166–188.
[19] H.M. Princen, Rheology of foams and highly concentrated emulsions, I. elastic properties and yield stress of a cylindrical model system, J. Colloid Interf. Sci. 91 (1) (1983) 160–175.
[20] I.M. Krieger, Rheology of monodisperse latices, Advances Colloid Interf. Sci. 3 (1972) 111–136.
[21] M.J. Mooney, The viscosity of a concentrated suspension of spherical particles, J. Colloid Sci. 6 (1951) 162–170.
[22] R. Pal, Rheology of polymer-thickened emulsions, J. Rheol. 36 (7) (1992).
[23] L.W. Lake, Enhanced Oil Recovery, Prentice Hall, New Jersey, 1989, p. 201–205.
[24] R.A. Nelson, Geologic Analysis of Naturally Fractured Reservoirs, second ed., Gulf Professional Publishing, 2001.
[25] R.O. Baker, A. Telesford, S. Wong, V. Li, G. Smith, H. Schoendorfer, An Integrated Fracture Characterization of a Heavy Oil Naturally Fractured carbonate Reservoir, paper no. 2001–13, Prepared for Presentation at the Petroleum Society's Canadian International Petroleum Conference held in Calgary, AB, Canada, 2001, pp.12–14.
[26] C.R. Wilson, An Investigation of Laminar Flow in Fractured Porous Rocks, Ph.D. Thesis, University of California, Berkeley, 1970.
[27] J.E. Gale, Comparison of coupled fracture deformation and fluid models with direct measurements of fracture pore structure and stress-flow properties, in: I.W., Farmer, J.J.K., Daemen, C.S., Desai, C.E., Glass, S.P., Neuman (Eds.), Rock Mechanics: Proceedings of the 28th US Symposium, Tucson, Arizona, Rotterdam, Balkema, Rotterdam, 1987, pp. 1213–1222.